Supporting Information

Holistic utilization of lignin-derived oligomers and polymers from oxidative catalysis to fabricate highly swelling agro-hydrogels

Zhichao Ma[a,b], Wenshuang Feng[b], Yuting Zhu[c], Xuhai Zhu[b], Haisong Wang[a,*], Ning Li[b,*], Feng Wang[b]

[a] Liaoning Key Lab of Lignocellulose Chemistry and BioMaterials, Liaoning Collaborative Innovation Center for Lignocellulosic Biorefinery, College of Light Industry and Chemical Engineering, Dalian Polytechnic University, Dalian 116034, China.

[b] Dalian National Laboratory for Clean Energy, Dalian Institute of Chemical Physics, Chinese Academy of Sciences, Dalian 116023, China.

Ning Li. Email: ningli603@dicp.ac.cn

Haisong Wang. Email: wanghs@dlpu.edu.cn

[c] Guangzhou Institute of Energy Conversion, Chinese Academy of Sciences, Guangzhou 510640, China.

Contents

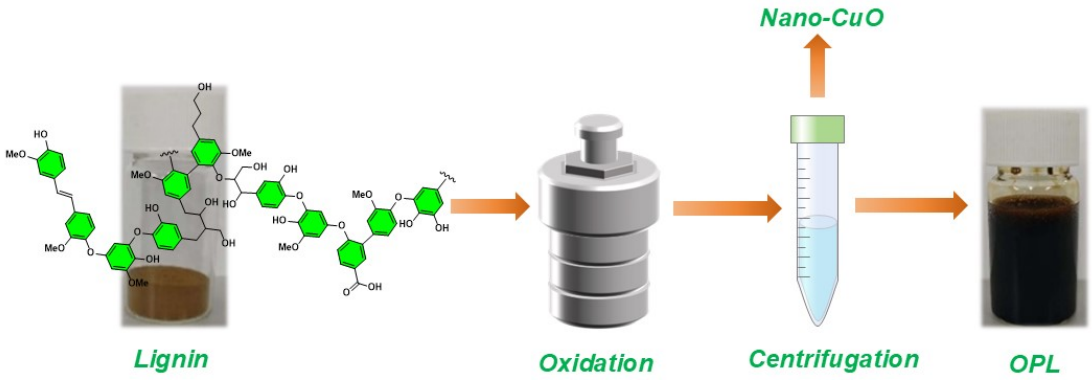

Fig. S1 Schematic illustration of the oxidation process of AL for the preparation of OPL.

The CuO nanoparticles were removed from the OPL by centrifugation.

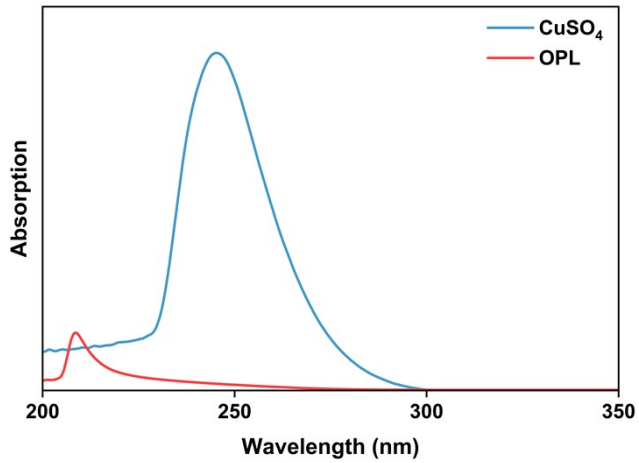

Fig. S2. UV assessment of residual copper in OPL ash.

2.0 g of OPL was calcined in a muffle furnace at 525 °C for 12 h to obtain the sample ash. 0.05 g of the ash was dissolved in 100 μL of 2 mol/L sulfuric acid, and the resulting solution was diluted to 40 mL with deionized water. After adjusting the solution pH to 6.5–7.0, 200 μL of 0.2 mol/L ethylenediamine solution was added as a chromogenic agent for Cu^{2+}. A 0.8 mol/L copper sulfate solution was used as the positive control; its pH was likewise adjusted to 6.5–7.0, followed by the addition of 200 μL of 0.2 mol/L ethylenediamine solution. Meanwhile, a copper-free blank solution (0.8 mol/L sulfuric acid, adjusted to pH 6.5–7.0 and mixed with 200 μL of 0.2 mol/L ethylenediamine solution) was prepared and used as the background reference for ultraviolet measurements.[1]

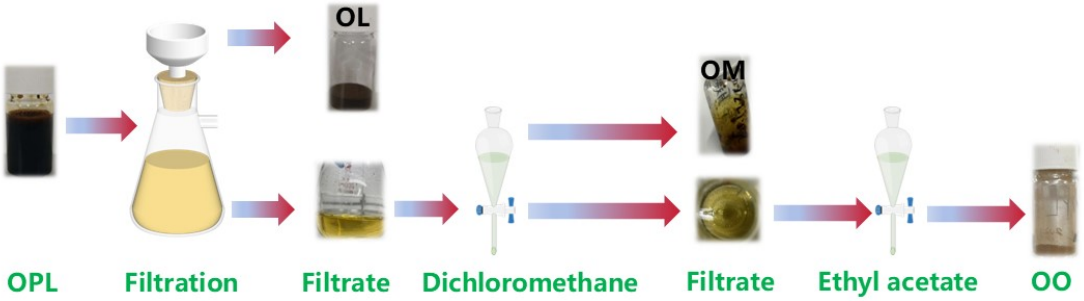

Fig. S3 Fractionation of OPL to yield OL, OM, and OO.

To separate OL, OO, and OM from OPL, the OPL mixture was acidified and filtered to obtain OL. The filtrate was extracted with dichloromethane (DCM) to isolate OM. After removing OM, the remaining aqueous phase was further extracted with ethyl acetate (EtOAc) to obtain OO. The detailed procedure is illustrated in Fig. S3.

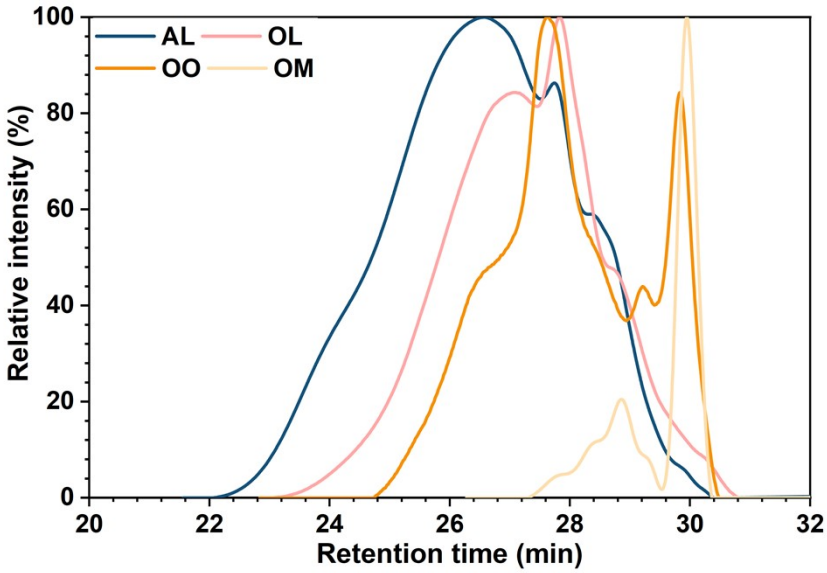

Fig. S4 Gel-permeation chromatography (GPC) traces of the different fractions obtained from the oxidation of alkaline lignin (AL).

Oxidation conditions: AL (0.5 g), CuO nanoparticles (0.5 g) and NaOH aqueous solution (7.5 wt%, 10 mL).

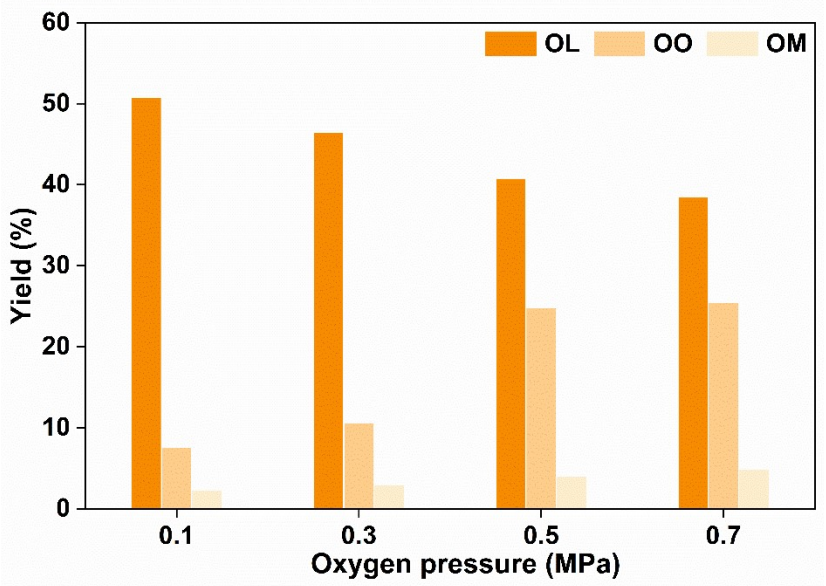

Fig. S5 Yields of OL, OO and OM at different oxygen pressures.

Oxidation conditions: AL (0.5 g), CuO nanoparticles (0.5 g) and NaOH aqueous solution (7.5 wt%, 10 mL).

With increasing oxygen pressure, the yield of OL decreased while the yields of OO and OM rose concomitantly. OO reached nearly 30% at 0.5 MPa. These results indicate that the oxidative protocol minimizes over-oxidation of AL, consistent with the experimental design. The oxidation of AL proceeds via stepwise reduction of molecular oxygen with concomitant electron transfer. Under alkaline conditions, this pathway generates reactive intermediates, notably the hydroperoxyl anion (HOO^-) and the superoxide radical anion ($O_2^{-}\cdot$).[2, 3] Initiation occurs through electrophilic attack of molecular oxygen on lignin's free phenolic hydroxyl groups. Electron abstraction from the resulting phenoxyl anion gives a phenoxyl radical and $O_2^{-}\cdot$. Proton-coupled electron transfer of $O_2^{-}\cdot$ then furnishes HOO^-.[4, 5] Superoxide ($O_2^{-}\cdot$), phenoxyl radicals, and HOO^- act as chain-propagating intermediates in lignin oxidation. Under higher oxygen pressure, their concentrations increase, thereby intensifying AL oxidation and shifting the product distribution toward higher OO and OM at the expense of OL.

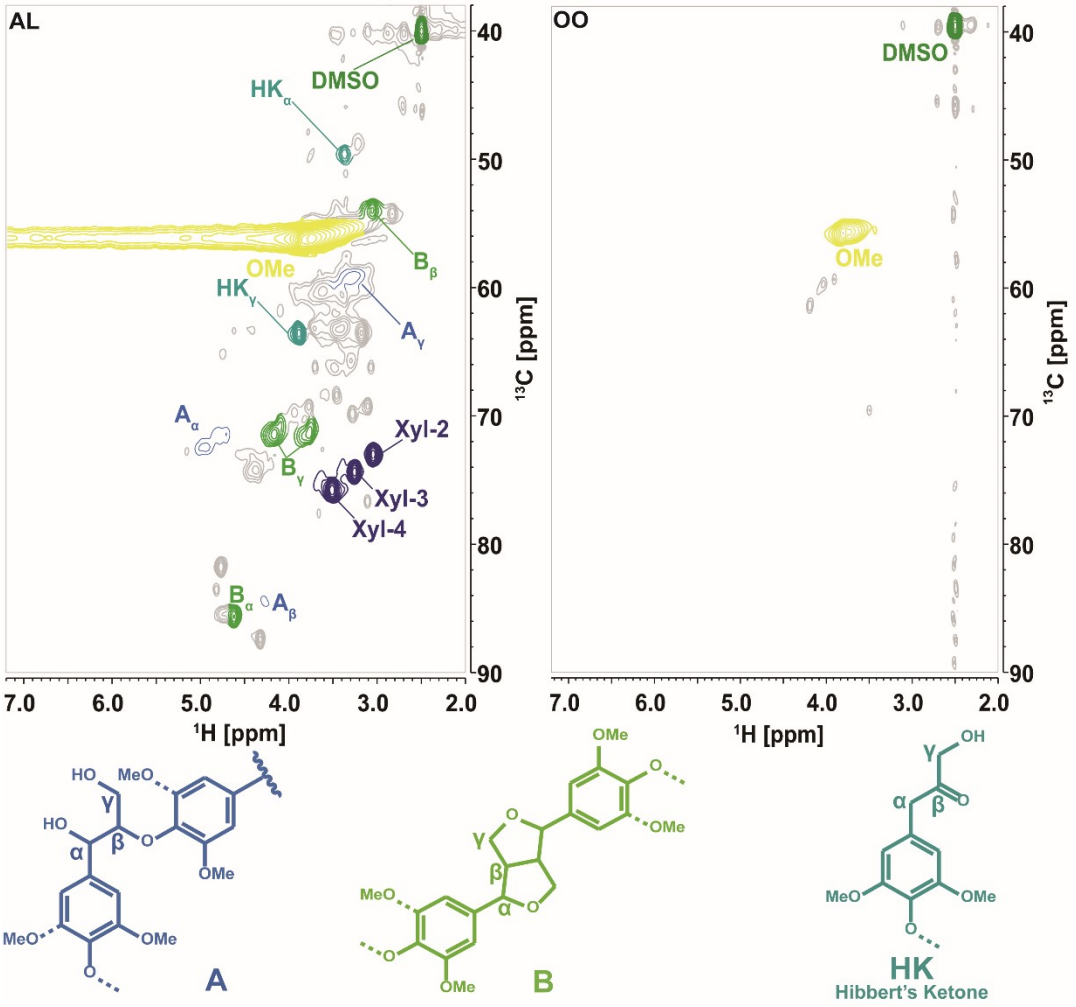

Fig. S6 HSQC NMR spectra of AL and OO in the aliphatic region.

Note: Signal assignments can be found in Table S2.[6-9]

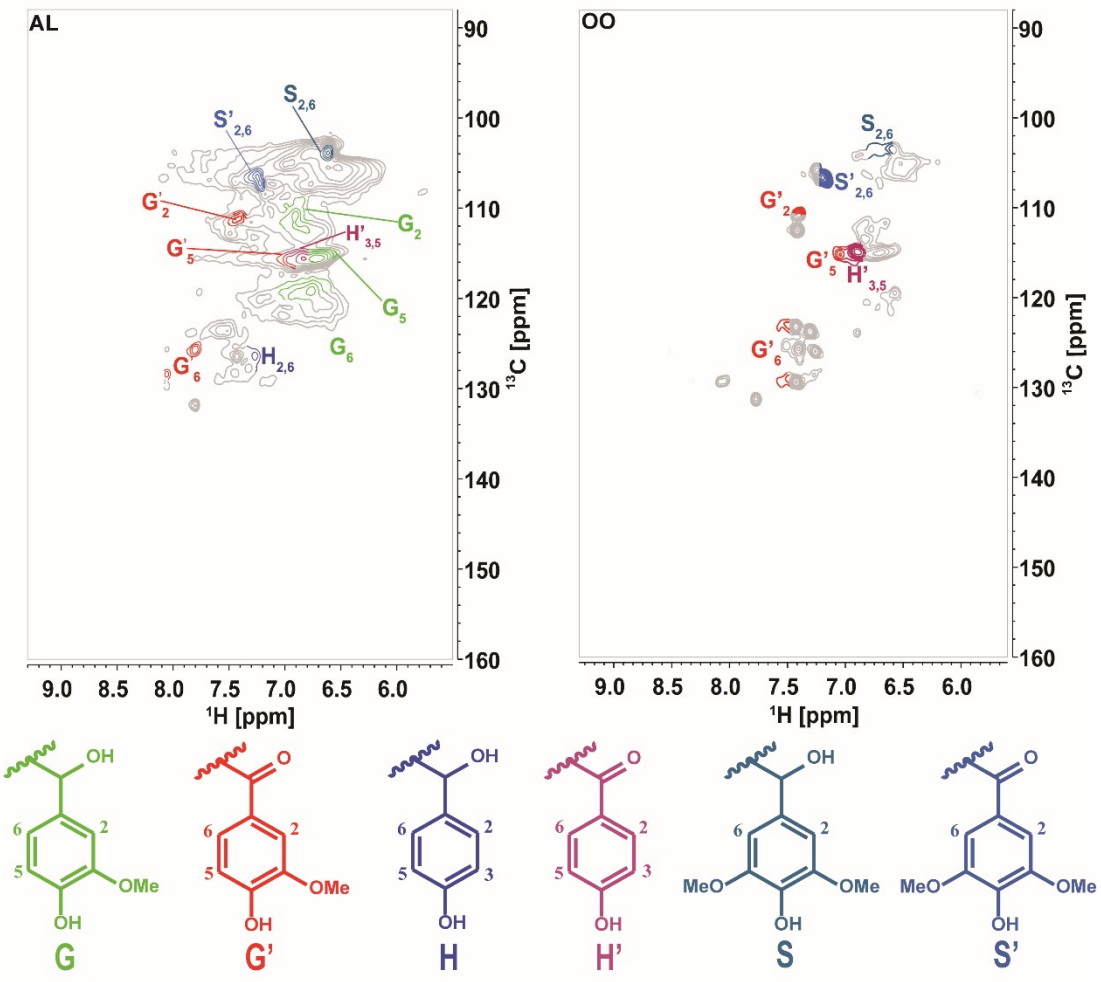

Fig. S7 HSQC NMR spectra of AL and OO in the aromatic region.

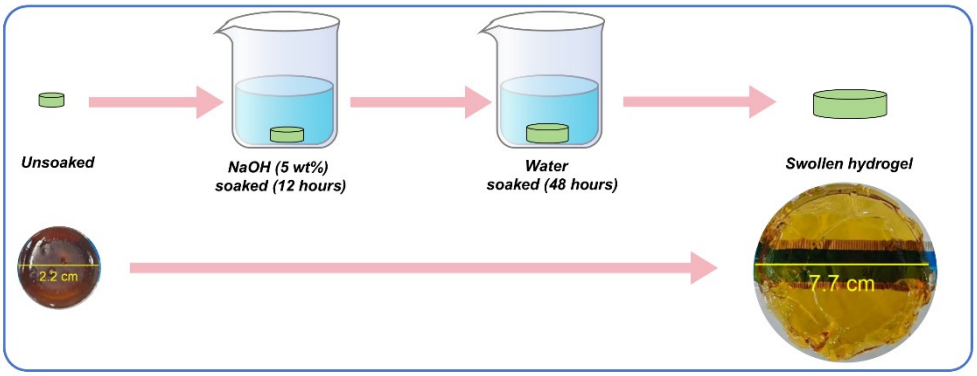

Fig. S8 Swelling behavior of OPLH.

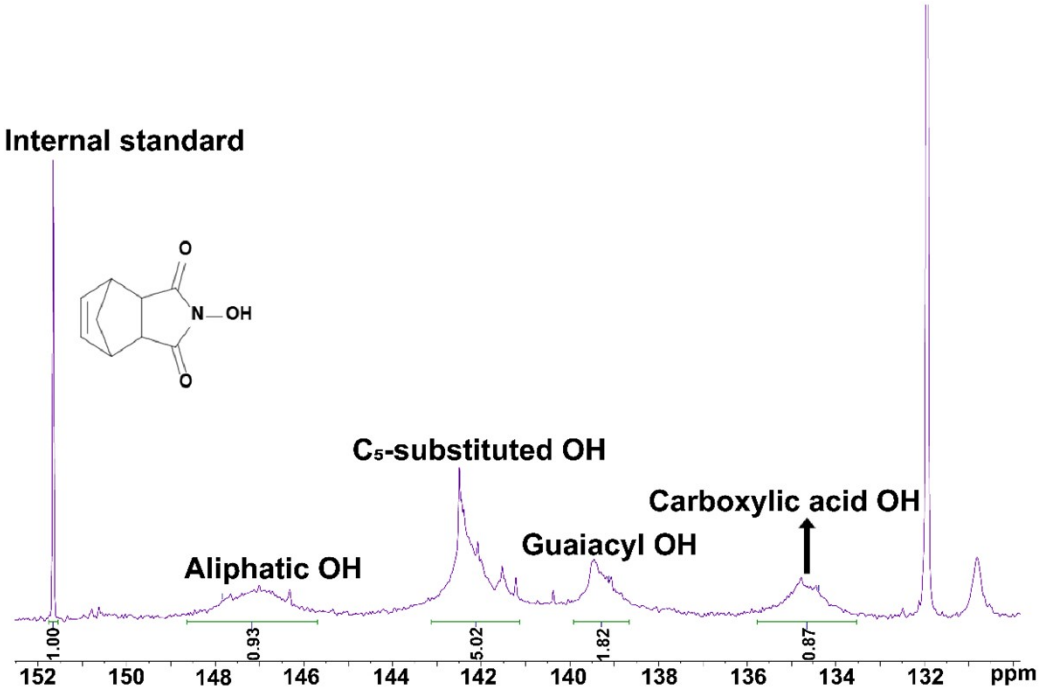

Fig. S9 ^{31}P NMR spectrum of OL.

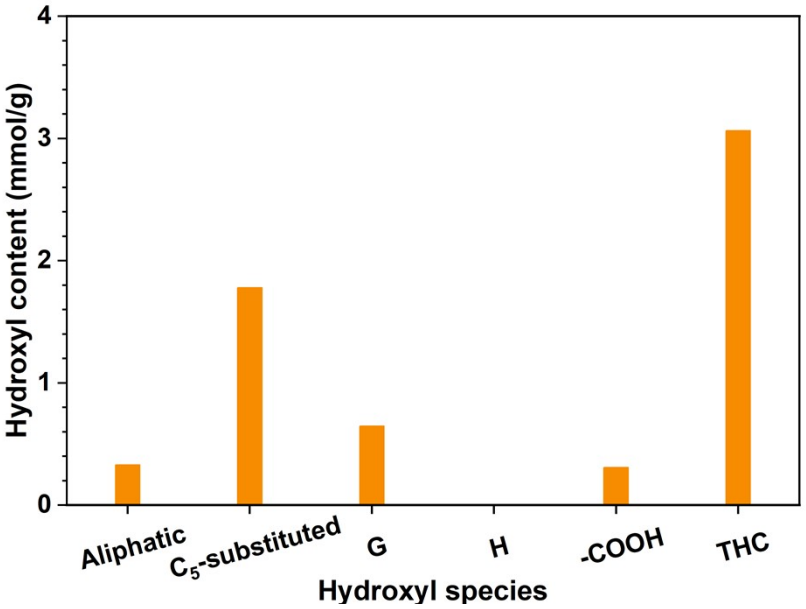

Fig. S10 Quantitation of various hydroxyl groups in OL by ^{31}P NMR. THC: total hydroxyl content.

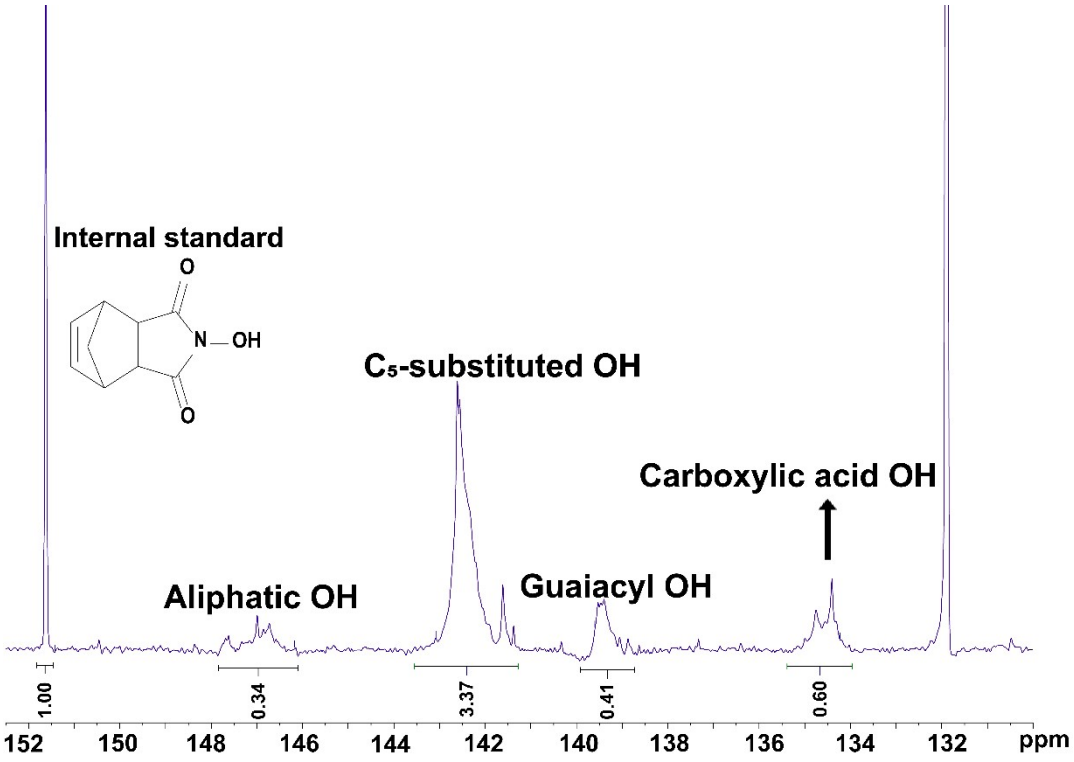

Fig. S11 ^{31}P NMR spectrum of AL.

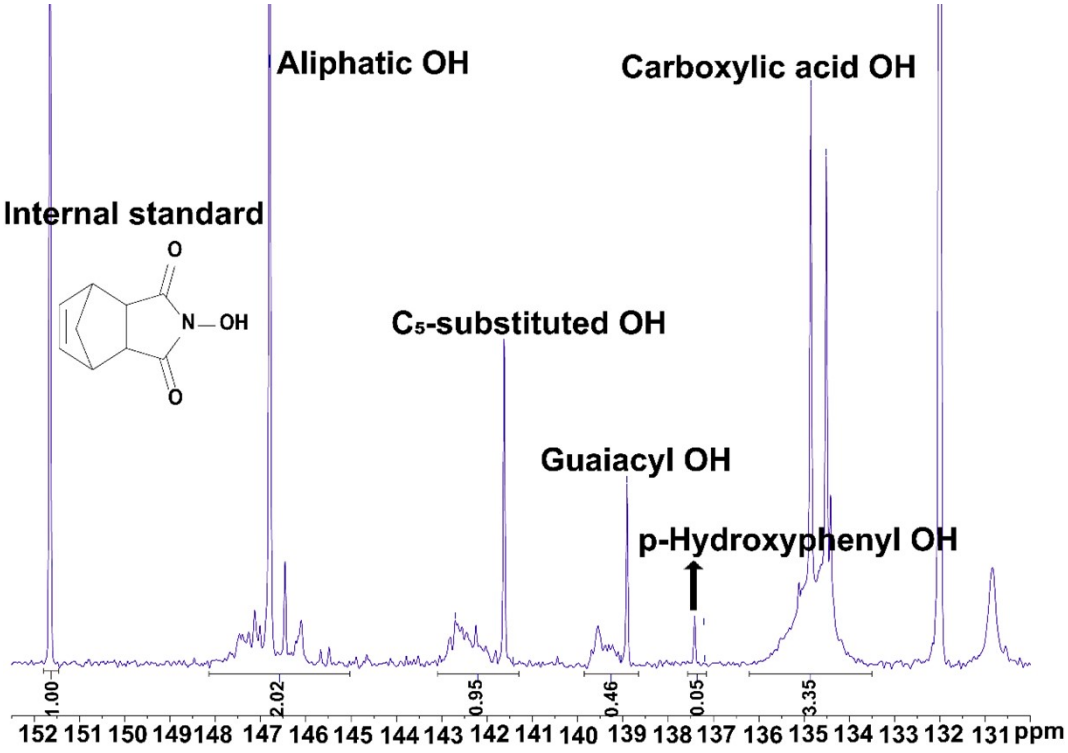

Fig. S12 ^{31}P NMR spectrum of OO.

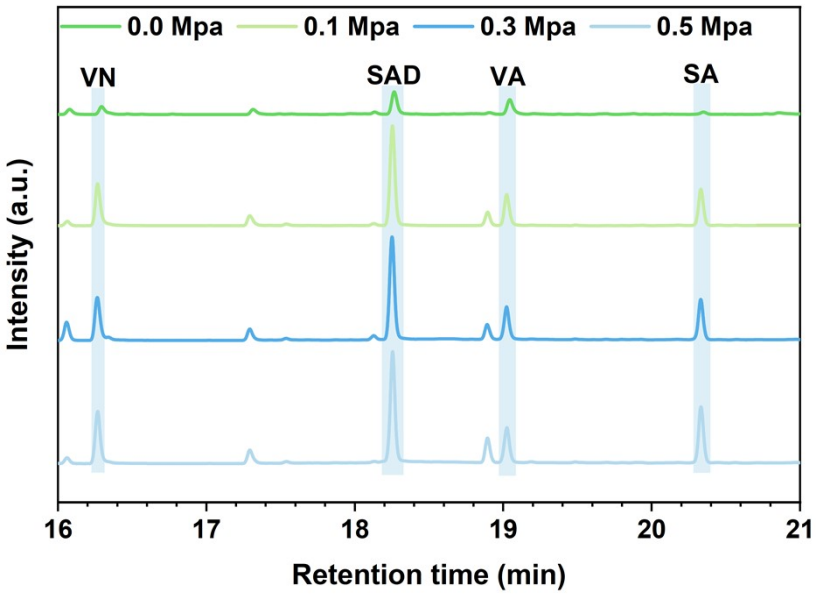

Fig. S13 Determination of aromatic monomers by GC-FID at different oxygen pressures.

Vanillin (VN), syringaldehyde (SAD), vanillic acid (VA), and syringic acid (SA).

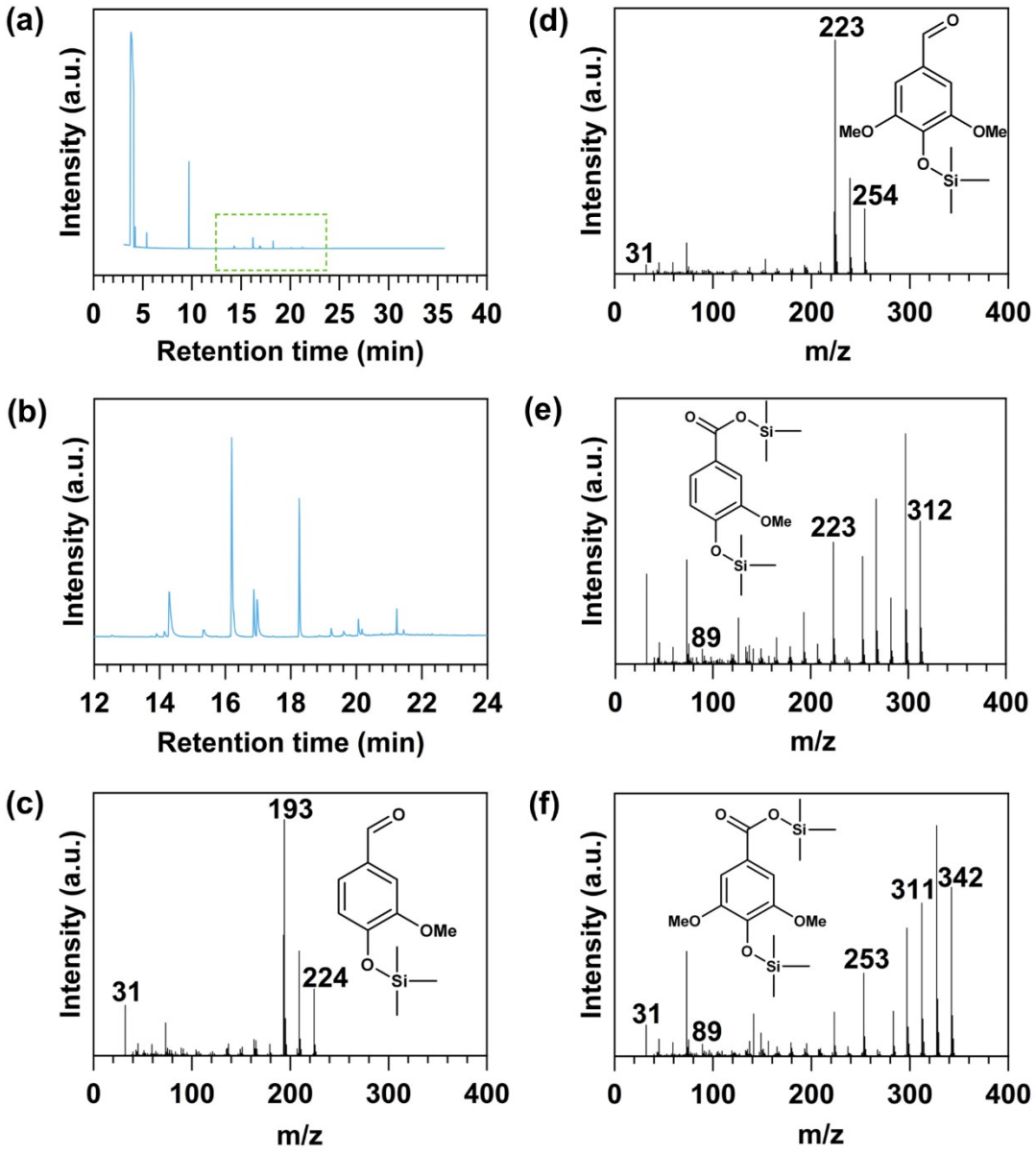

Fig. S14 Identification of the aromatic monomers in the organic phase of the OPL filtrate.

(a) GC-MS spectrum of the dichloromethane phase (0-40min), (b) GC-MS spectrum of the dichloromethane phase, (c) MS spectrum of VN, (d) MS spectrum of SAD, (e) MS spectrum of VA, (f) MS spectrum of SA.

The filtrate obtained after lignin oxidation is dominated by four monophenols: VN, VA, SAD, and SA (Fig. S14).

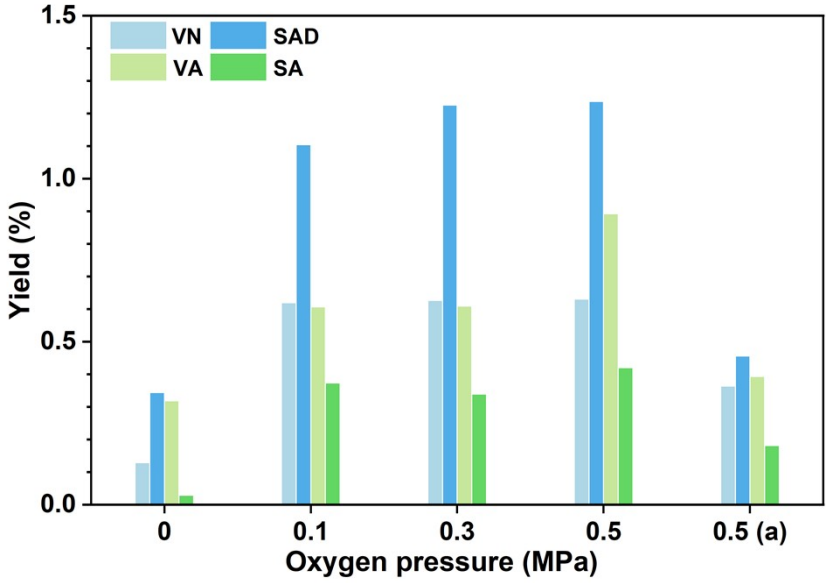

Fig. S15 Yields of VA, VN, SAD, and SA at different oxygen pressures.

Note: 0.5 MPa denotes the condition without CuO nanoparticles.

The monophenol yields increase progressively with oxygen pressure, with syringaldehyde predominating (Fig. S15). Data at 0 and 0.5 MPa indicate that mild lignin oxidation arises from the combined effect of low-pressure oxygen and copper oxide nanoparticles.

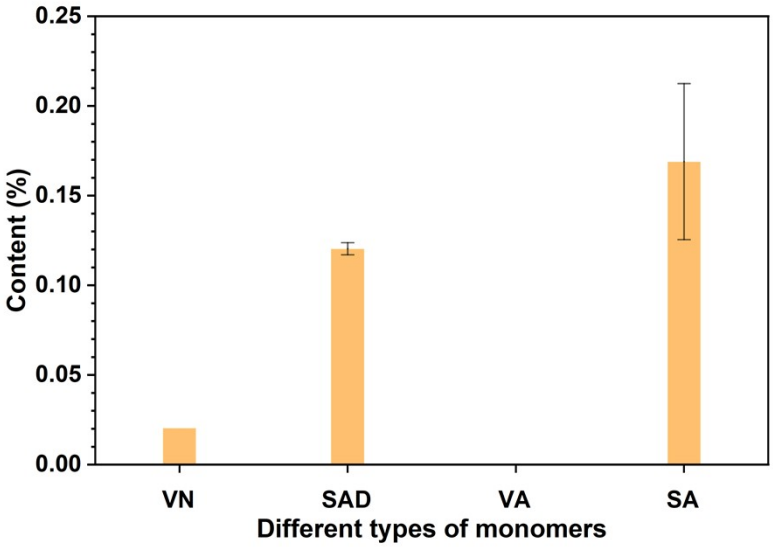

Fig. S16 Monophenol content in oligomers.

All experimental results shown in the figures are based on parallel experiments performed with at least three replicates ($n \geq 3$).

The oligomers obtained via the separation procedure outlined in Fig. S3 are characterized by only trace amounts of monomers, with the highest SA content reaching 0.2% (Fig. S16). Notably, the reported yield of 24.8% refers to the monomer fraction within the oligomers; when calculated relative to the initial 0.5 g of lignin, the yield is lower. These results indicate that the oligomers obtained by this method are of high purity, with monomeric species present at levels insufficient to influence the properties of the resulting oligomeric hydrogels.

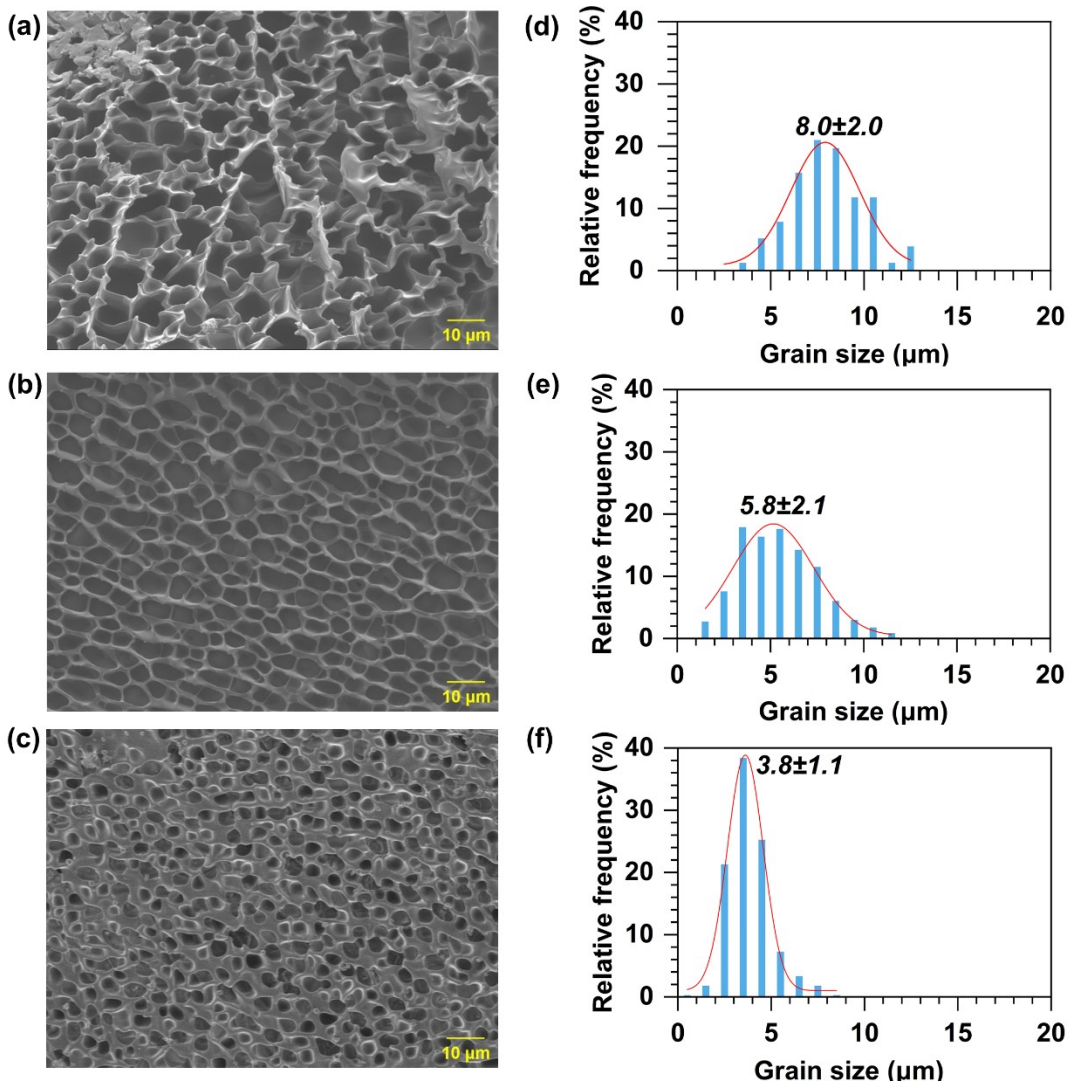

Fig. S17 Surface morphologies and pore size distributions of the hydrogels.

Figures (a–c) show the surface morphology of the hydrogels, while figures (d–f) depict their pore size distributions. The samples are labeled as follows: (a, d) PAAH; (b, e) ALH–X; (c, f) (OL+OO)H–X (X=3.4 wt%). Here, ALH–X and (OL+OO)H–X indicate hydrogels containing X wt% of AL and OL+OO, respectively.

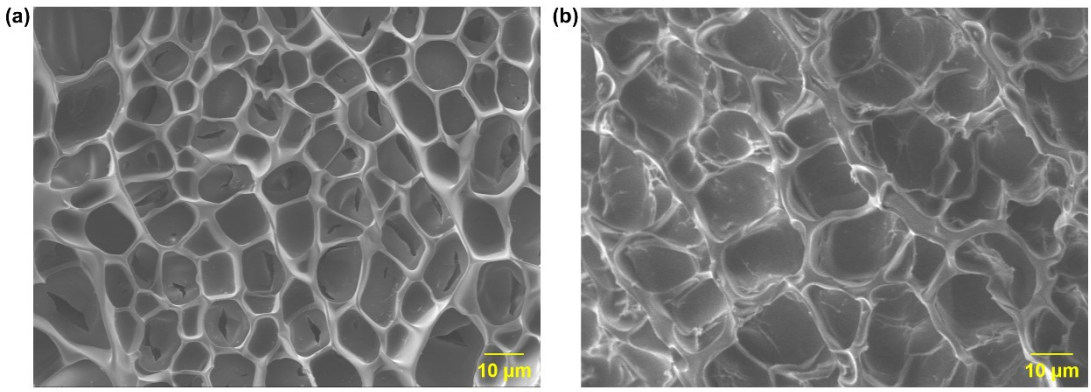

Fig. S18 Surface morphology of OMH–X (X=3.4 wt%).

Figures (a, b) show the surface morphology of the OMH–X hydrogel, where OMH–X denotes a hydrogel containing X wt% of OM.

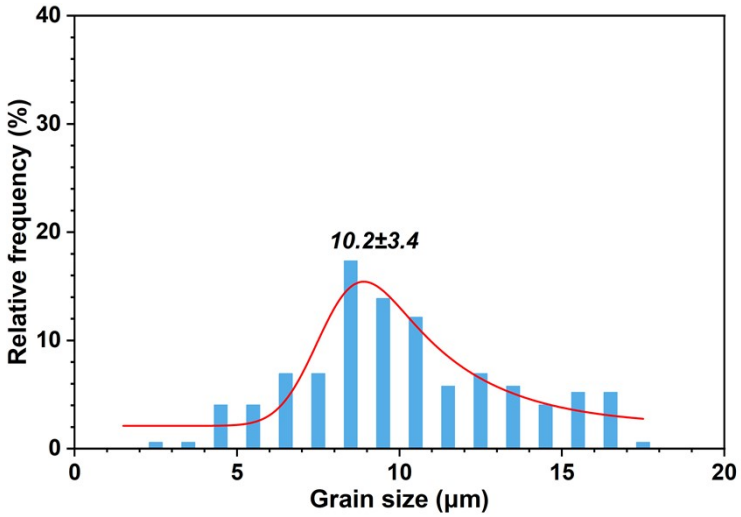

Fig. S19 Pore size distribution of OMH–X (X=3.4 wt%).

OMH–X denotes a hydrogel containing X wt% of OM.

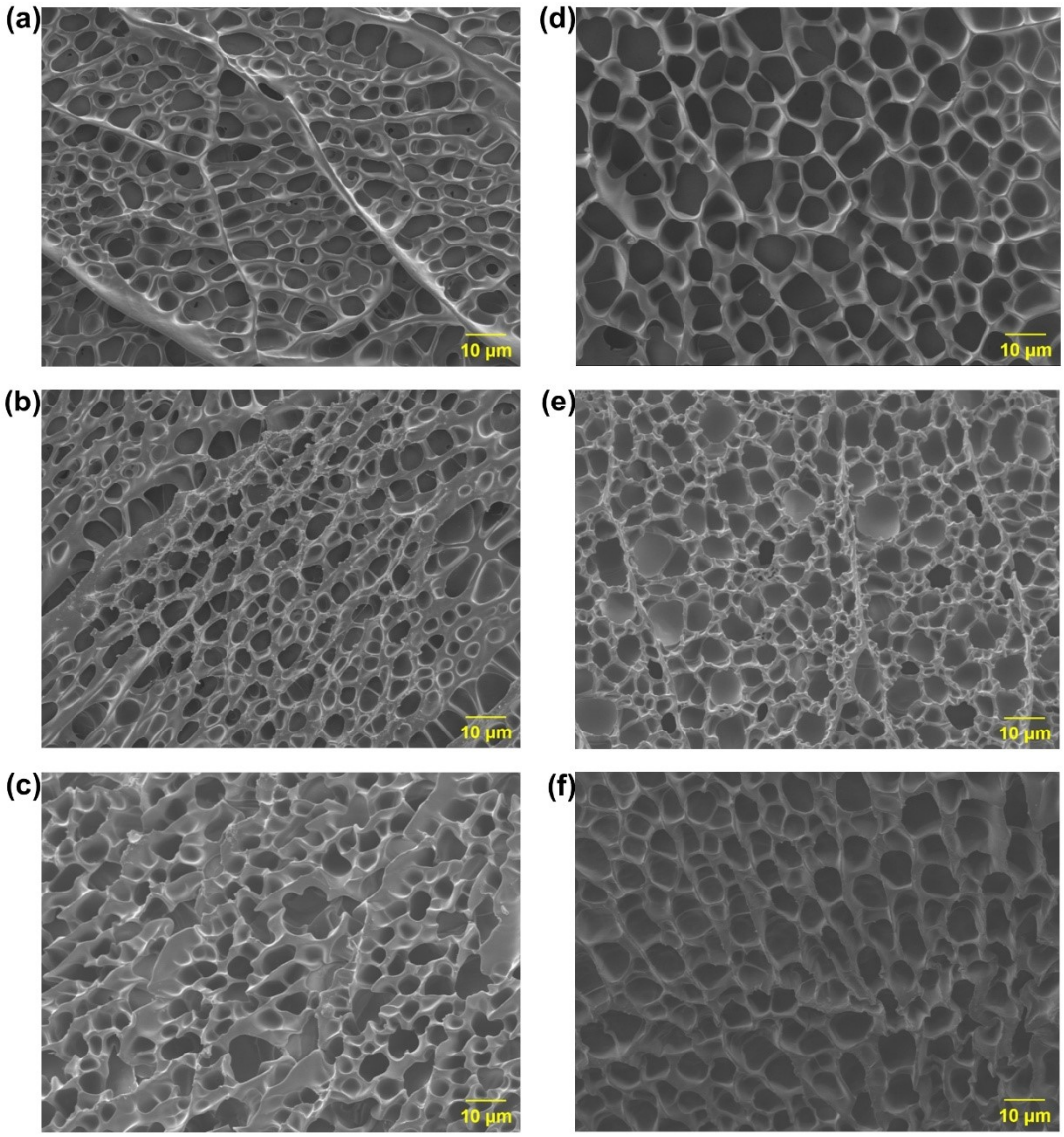

Fig. S20 Surface morphologies of lignin-containing hydrogels with varied loadings.

The samples are labeled as follows: (a) OPLH–0.9, (b) OPLH–1.7, (c) OPLH–2.5, (d) ALH–0.9, (e) ALH–1.7, and (f) ALH–2.5 hydrogels. Here, ALH–X and OPLH–X denote hydrogels containing X wt% of AL and OPL, respectively.

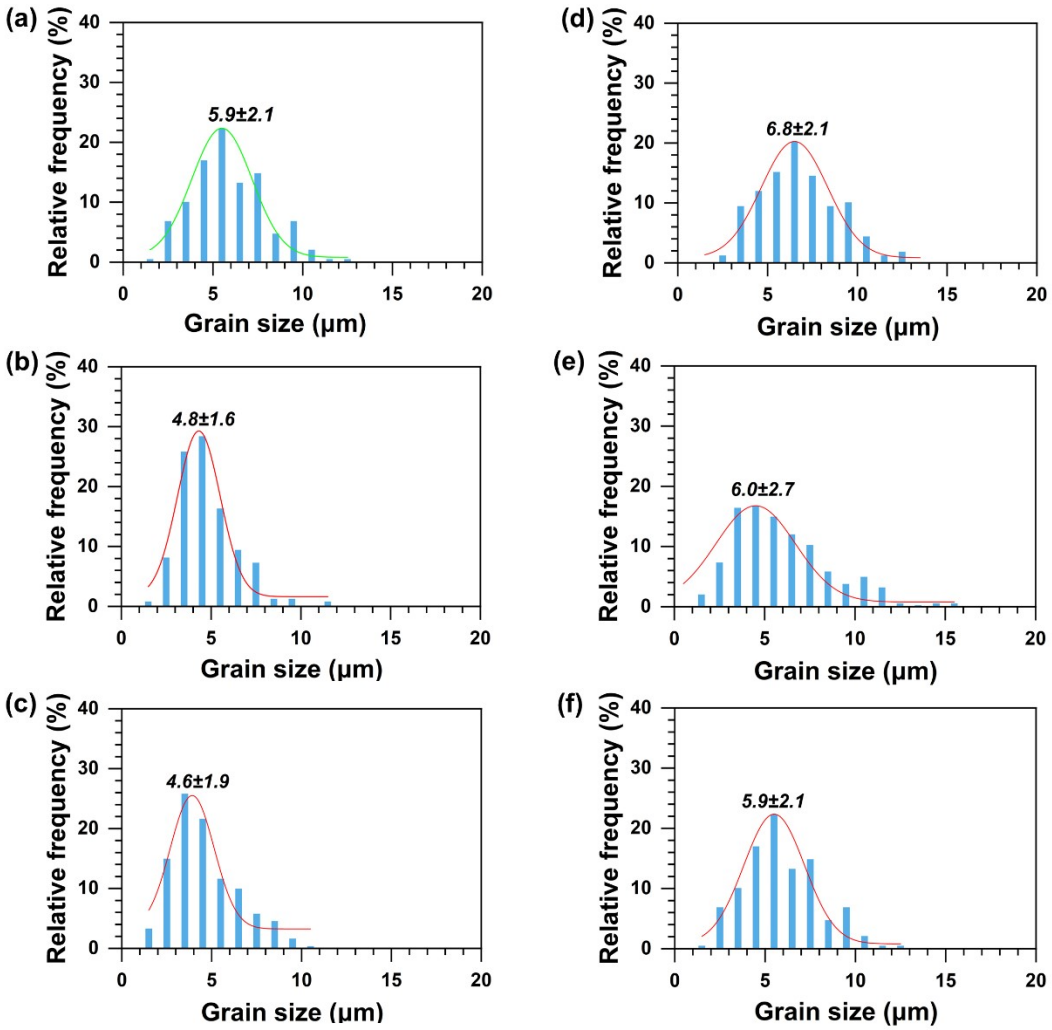

Fig. S21 Pore size distributions of ALH–X and OPLH–X.

Figures (a–f) correspond to: (a) OPLH–0.9, (b) OPLH–1.7, (c) OPLH–2.5, (d) ALH–0.9, (e) ALH–1.7, and (f) ALH–2.5. Here, ALH–X and OPLH–X denote hydrogels containing X wt% AL and OPL, respectively.

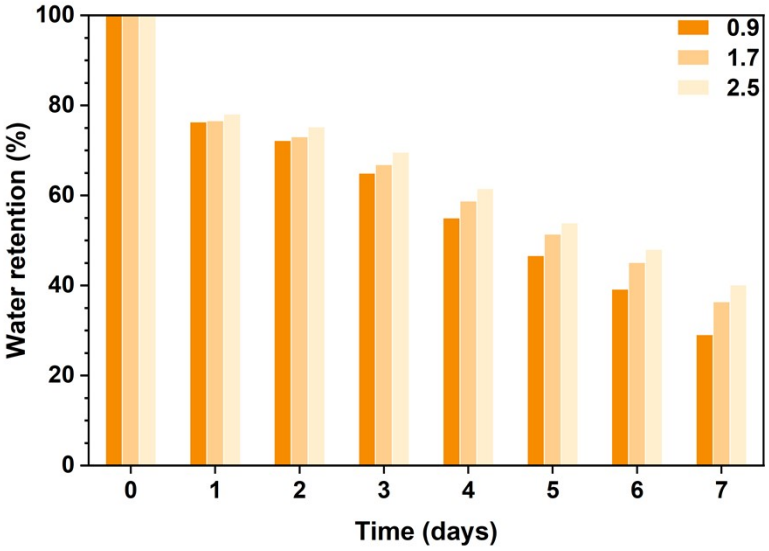

Fig. S22 Water retention capacity of ALH–X in soil.

ALH–X (X=0.9, 1.7, 2.5) denotes hydrogels prepared with X wt% AL.

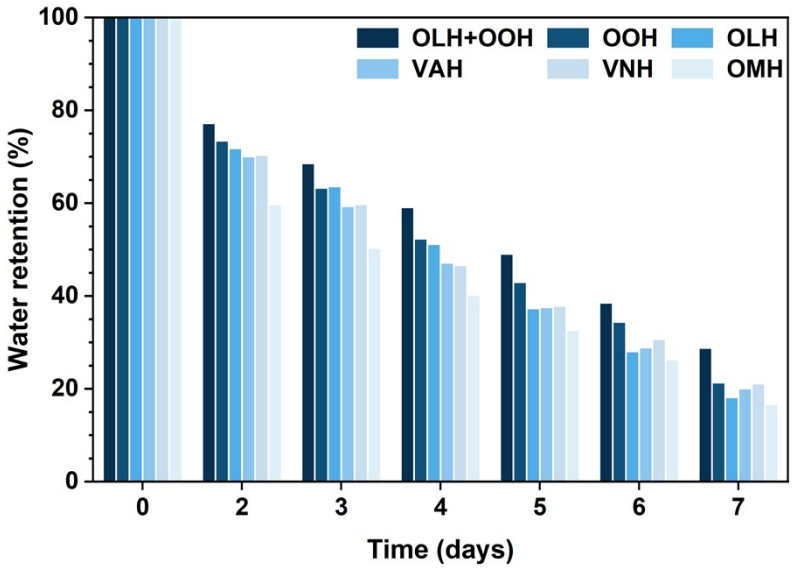

Fig. S23 Effect of different hydrogels on water retention in sandy soil.

(OL+OO)H–X, OOH–X, OLH–X, VAH–X, VNH–X and OMH–X (X=3.4) refer to hydrogels prepared with X wt% of OL+OO, OO, OL, VA, VN and OM, respectively.

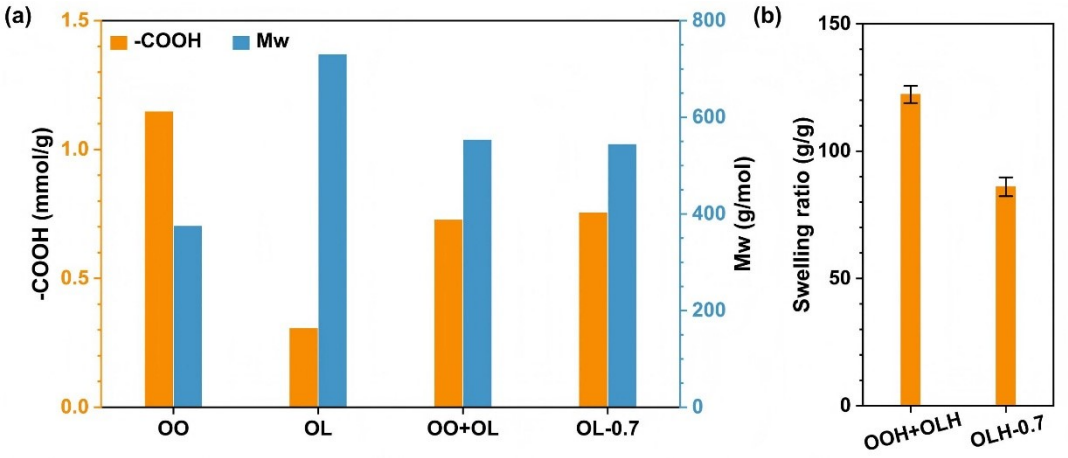

Fig. S24. Comparison of the carboxyl content and weight-average molecular weight (Mw) of OL+OO and OL-0.7 MPa, and comparison of the swelling ratio of the corresponding hydrogels.

(a) Carboxyl content and Mw of OL+OO and OL-0.7 MPa. (b) Swelling ratio of (OL+OO)H and OLH-0.7 MPa. OL-0.7 denotes OL prepared under an oxygen pressure of 0.7 MPa. (OL+OO)H refers to the hydrogel prepared using OO and OL at a feeding ratio of OO:OL = 0.0204 g: 0.0196 g, whereas OLH-0.7 MPa denotes the hydrogel prepared from 0.04 g of OL-0.7.

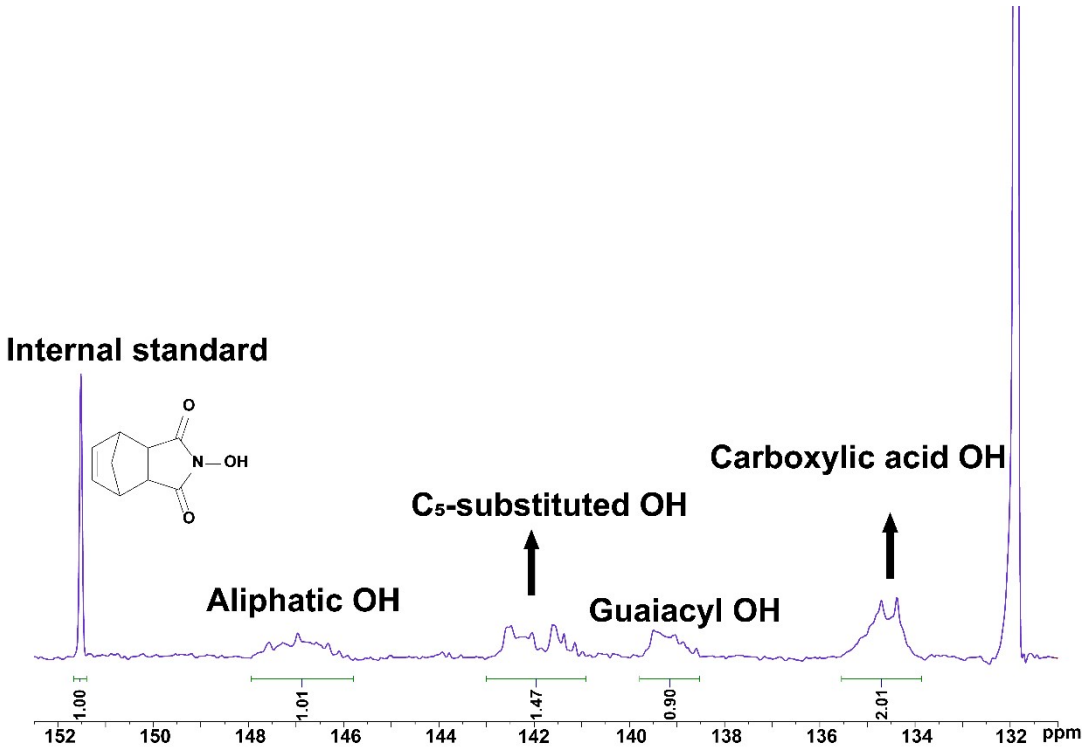

Fig. S25 ^{31}P NMR spectrum of OL-0.7.

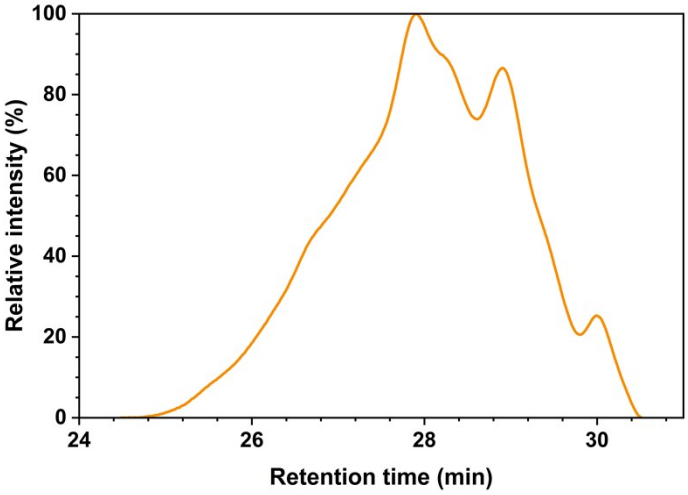

Fig. S26 GPC chromatogram of OL-0.7.

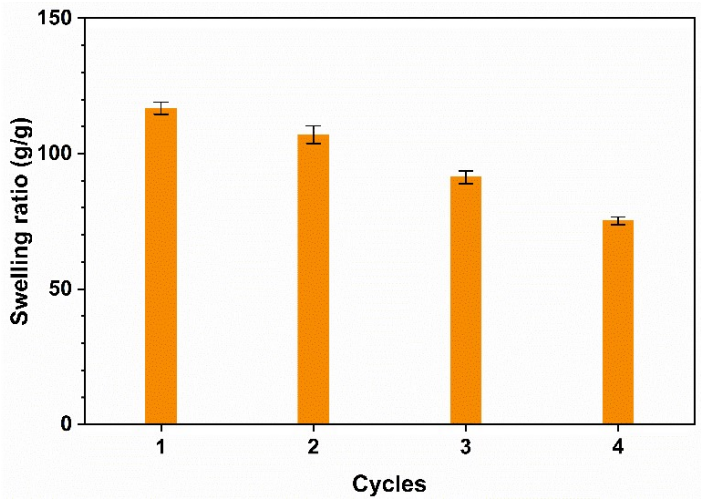

Fig. S27. Repeated swelling–drying cycles of OPLH.

OPLH was fabricated using OPL prepared under an oxygen pressure of 0.5 MPa, with an OPL loading of 3.4 wt%. Repeated swelling–drying cycles were performed on OPLH: OPLH was first freeze-dried in a freeze dryer, and then the dried gel was immersed in deionized water. The mass before and after immersion was recorded, and the swelling ratio was calculated according to Equation (3). The above cycles were repeated four times.

$$w_r = (m_b - m_a)/(m_a) \quad (3)$$

where w_r is the water absorption and swelling ratio of the hydrogel, m_b is the mass of the swollen hydrogel, and m_a is the initial mass of the dried hydrogel.

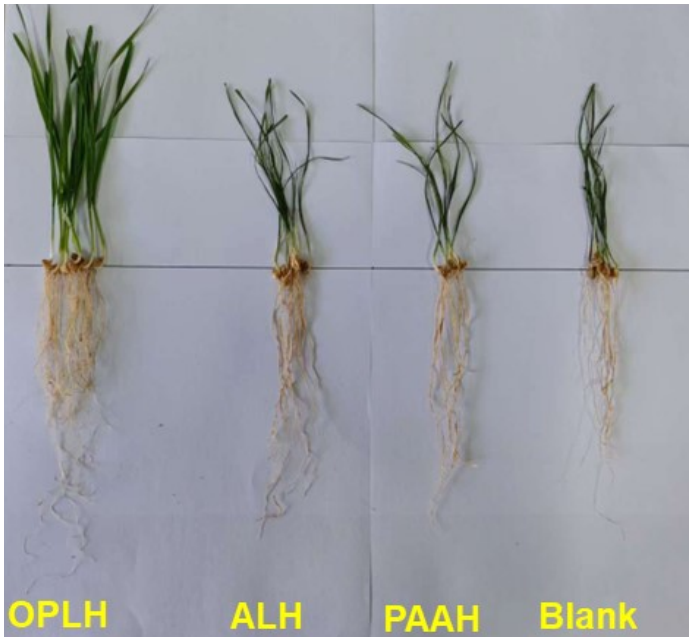

Fig. S28 Barley growth in sandy soil containing various hydrogels, 8 days post-planting.

All data shown are from parallel experiments with a minimum of six replicates ($n \geq 6$).

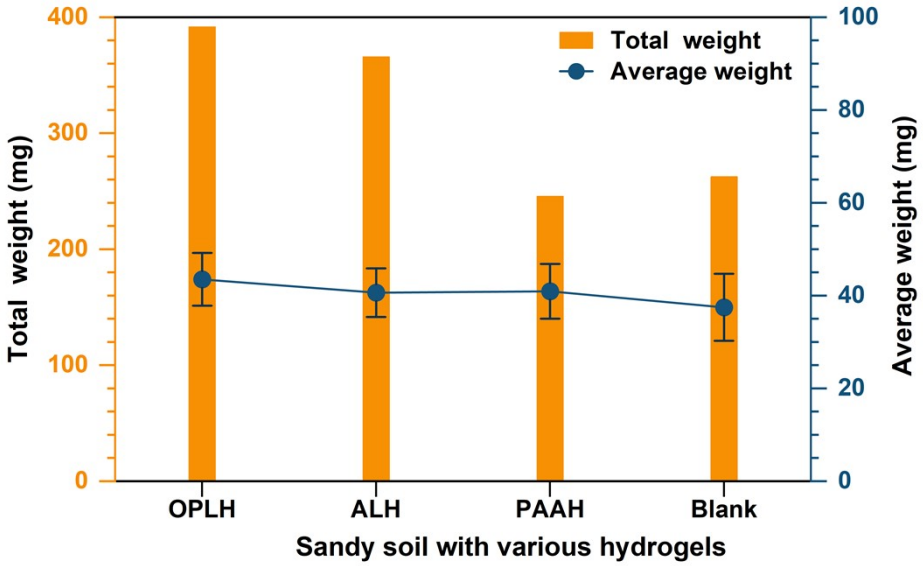

Fig. S29 Hydrogel impact on barley growth: average and total dry weight, 8 days post-planting.

All data shown are from parallel experiments with a minimum of six replicates ($n \geq 6$).

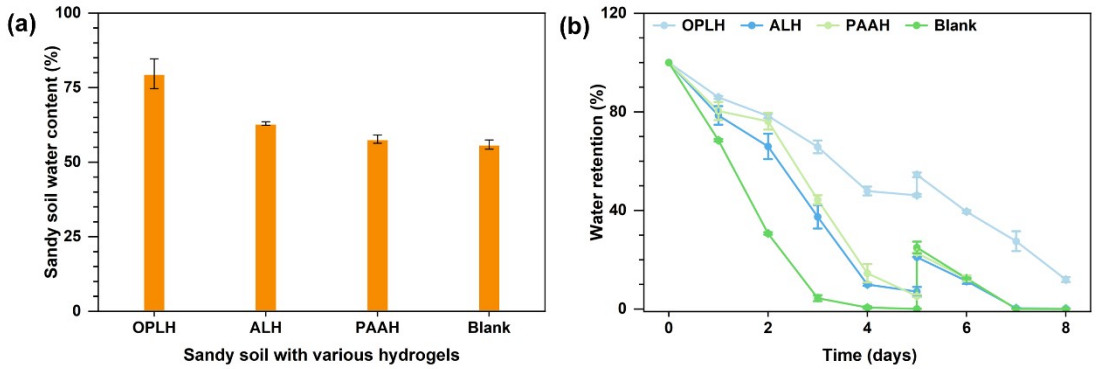

Fig. S30 Water-content dynamics in sandy soil with various hydrogels after barley planting.

(a) Initial water content of hydrogel-amended sandy soil at barley planting. (b) Temporal changes in soil water content over the subsequent eight days (days 1–8).

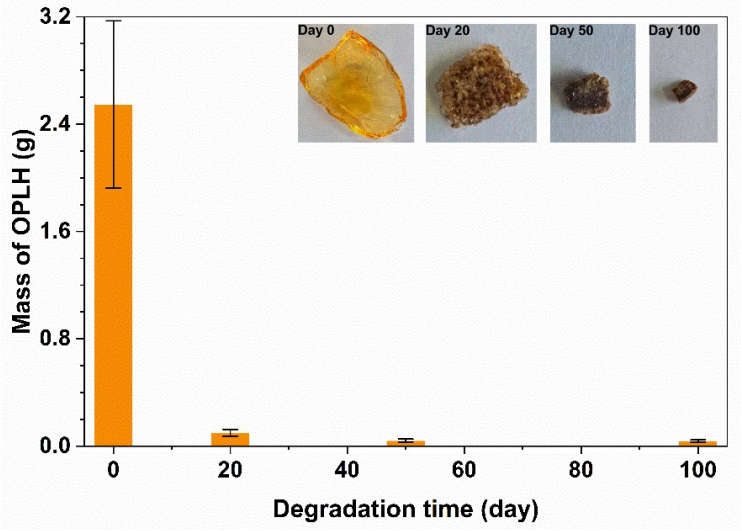

Fig. S31. Degradation of OPLH in soil.

The experimental method was adapted from Song et al.[10] First, 20 g of swollen hydrogel was buried in a plastic culture box containing 20 g of sandy soil. An additional 20 g of sandy soil was then uniformly covered over the hydrogel surface. The samples were retrieved and weighed at 0, 20, 50, and 100 days after burial, respectively. The sandy soil used in this experiment was the same as that employed in the barley cultivation experiment.

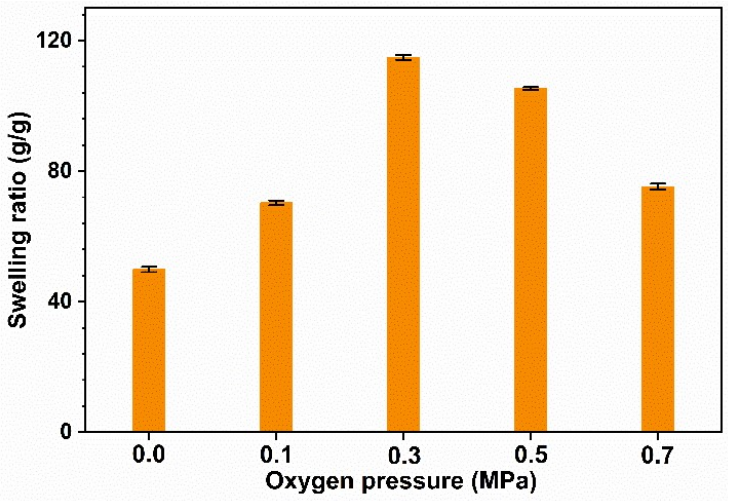

Fig. S32. Swelling ratios of OPLH prepared under different oxygen pressures.

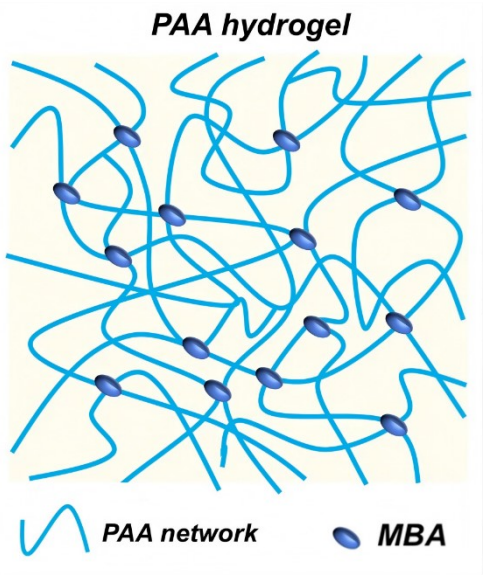

Fig. S33. Proposed polymer network of PAAH.

Table S1 Formulation parameters of the synthesized hydrogels.

Hydrogel	PAA (g)	Other components
OPLH	—	OPL (wt %)
	1	0.9
	1	1.7
	1	2.5
	1	3.4
ALH	—	AL (wt %)
	1	0.9
	1	1.7
	1	2.5
	1	3.4
(OL+OO)H	—	OL+ OO (wt %)：
	1	3.4
	1	4.0
OLH	—	OL (wt %)
	1	3.4
OOH	—	OO (wt %)
	1	3.4
OMH	—	OM (wt %)
	1	3.4
VNH	—	VN (wt %)
	1	3.4
VAH	—	VA (wt %)
	1	3.4
PAAH	1	—

ALH was prepared by dissolving 0.5 g of AL in 10 mL of a 7.5 wt% NaOH solution. (OL+OO)H was synthesized using mixtures of OO and OL at mass ratios of 1:1 and 0.0204: 0.0196 (w/w), respectively, following the same preparation procedure as ALH. OLH was prepared using not only OL obtained at an oxygen pressure of 0.5 MPa, but also OL treated at 0.7 MPa (denoted as OL-0.7). OPLH was synthesized with OPL prepared at oxygen pressures of 0, 0.1, 0.3, 0.5, and 0.7 MPa, respectively. All other raw materials were prepared under an oxygen pressure of 0.5 MPa. OOH, OLH, OMH, VNH and VAH were synthesized following the ALH protocol, with the corresponding components incorporated at the specified weight percentages.

Table S2 Summary of assignments for key ^{13}C–^{1}H cross-peaks in the HSQC spectra.

Labels	δC/δH (ppm)	Assignments
A_α(G)	71.07/4.74	C_α–H_α in β–O–4 substructures linked to G unit (A)
A_β(G/H)	83.47/4.29	C_β–H_β in β–O–4 substructures linked to G/H (A)
A_γ	60/3.3 and 3.6	C_γ–H_γ in β–O–4 substructures (A)
B_α	85.19/4.66	C_α–H_α in β–β(resinol) (B)
B_β	53.45/3.09	C_β–H_β in β–β (resinol) (B)
B_γ	71.08/3.84 and 4.2	C_γ–H_γ in β–β (resinol) (B)
G_2	110.81/6.98	C_2–H_2 in guaiacyl units (G)
G_6	118.67/6.78	C_6–H_6 in guaiacyl units (G)
G_5	114.85/6.76	C_5–H_5 in guaiacyl units (G)
G'_2	110.57/7.37	C_2–H_2 in Cα=O oxidized guaiacyl units (G')
G'_6	122.7-128.6/6.8-7.6	C_6–C_6 in Cα=O oxidized guaiacyl units (G')
G'_5	115.44/7.02	C_5–H_5 in Cα=O oxidized guaiacyl units (G')
$H_{2,6}$	127.72/7.2	$C_{2,6}$–$H_{2,6}$ in H units (H)
$H'_{3,5}$	114.97/6.87	$C_{3,5}$–$H_{3,5}$ in Cα=O oxidized H units (H')
$S_{2,6}$	103.6/6.65	$C_{2,6}$–H,6_2 in syringyl units (S)
$S'_{2,6}$	106.32/7.16 and 7.34	$C_{2,6}$–$H_{2,6}$ in oxidized syringyl units (S')

References

1. T. Wen, F. Qu, N. B. Li and H. Q. J. A. J. o. C. Luo, A facile, sensitive, and rapid spectrophotometric method for copper(II) ion detection in aqueou s media using polyethyleneimine, *Arabian Journal of Chemistry*, 2017, **10**.
2. R. Ma, Y. Xu and X. Zhang, Back cover: catalytic oxidation of biorefinery lignin to value-added chemicals to support sustainable biofuel production, *ChemSusChem*, 2015, **8**, 194-194.
3. L. Passauer, K. Fischer and F. Liebner, Activation of pine Kraft lignin by Fenton-type oxidation for cross-linking with oligo (oxyethylene) diglycidyl ether, *Holzforschung*, 2011, **65**, 319-326.
4. R. Yang, L. Lucia, A. J. Ragauskas and H. Jameel, Oxygen delignification chemistry and its impact on pulp fibers, *J. Wood Chem. Technol.*, 2003, **2 3**, 13-29.
5. S. Fu, J. M. Singh, S. Wang and L. A. Lucia, Investigation of the chemis try of oxygen delignification of low Kappa softwood Kraft pulp using an organic/Inorganic chemical selectivity system, *J. Wood Chem. Technol.*, 20 05, **25**, 95-108.
6. M.-K. He, Y.-L. He, Z.-Q. Li, L.-N. Zhao, S.-Q. Zhang, H.-M. Liu and Z. Qin, Structural characterization of lignin and lignin-carbohydrate complex (LCC) of sesame hull, *Int. J. Biol. Macromol.*, 2022, **209**, 258-267.
7. J.-L. Wen, S.-L. Sun, B.-L. Xue and R.-C. Sun, Recent advances in chara cterization of lignin polymer by solution-state nuclear magnetic resonance (NMR) methodology, *Materials*, 2013, **6**, 359-391.
8. J. Rencoret, G. Marques, A. Gutiérrez, L. Nieto, J. Jiménez-Barbero, Á. T. Martínez and J. C. del Río, Isolation and structural characterization of the milled-wood lignin from Paulownia fortunei wood, *Ind. Crop. Prod.*, 2009, **30**, 137-143.
9. J. Zeng, G. L. Helms, X. Gao and S. Chen, Quantification of wheat straw lignin structure by comprehensive NMR analysis, *J. Agric. Food Chem.*, 2 013, **61**, 10848-10857.
10. B. S. A, H. L. A, R. S. A, P. P. B, Y. J. C and D. S. D. J. I. J. o. B. M. E, Hydrogel synthesis based on lignin/sodium alginate and application i n agriculture, *International Journal of Biological Macromolecules*, 2020, **14 4**, 219-230.